chemengineering

Supplementary Material: Electrochemical synthesis-dependent photoelectrochemical properties of tungsten oxide powders

Anastasia Tsarenko, Mikhail Gorshenkov, Aleksey Yatsenko, Denis Zhigunov, Vera Butova, Vasily Kaichev and Anna Ulyankina

Table S1. Fitting data of XRD patterns of WO_3 samples using MAUD software.

Sample	Lattice parameters [Å]	ICSD entry
WO_3-OA	WO_3 P $2_1/n$ a = 7.316(5) b = 7.512(8) c = 7.683(3) β = 90.56(9)	
WO_3-SA	WO_3 P $2_1/n$ a = 7.323(3) b = 7.510(1) c = 7.678(7) β = 90.47(2)	80056 P $2_1/n$ a = 7.30084(7) b = 7.53889(7) c = 7.68962(8) β = 90.892(1)
WO_3-NA	WO_3 P $2_1/n$ a = 7.346(3) b = 7.536(9) c = 7.7063(1) β = 90.44(6)	

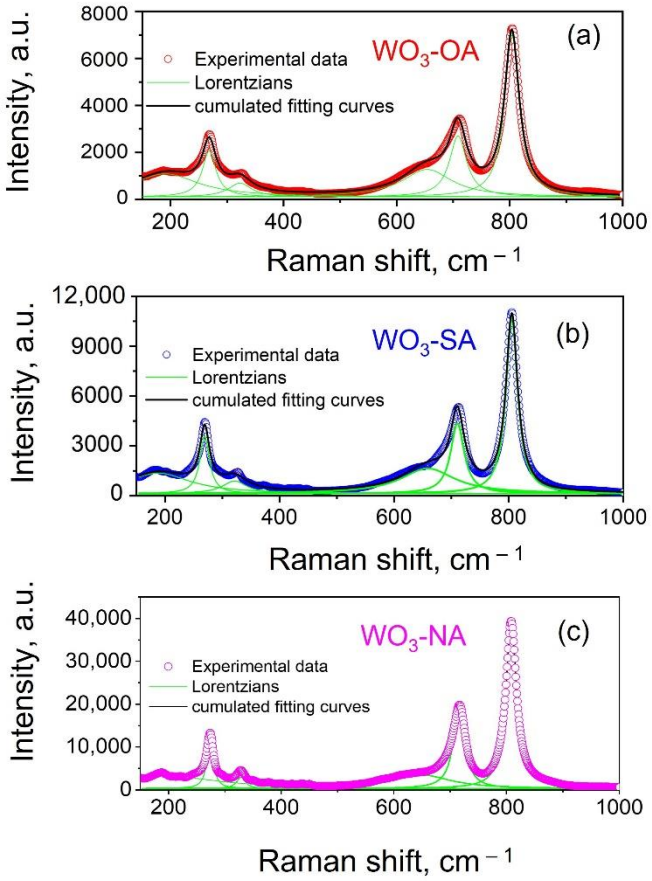

Figure S1. Lorentzian curve fitting for Raman spectra of WO_3-OA (**a**), WO_3-SA (**b**) and WO_3-NA (**c**) samples.

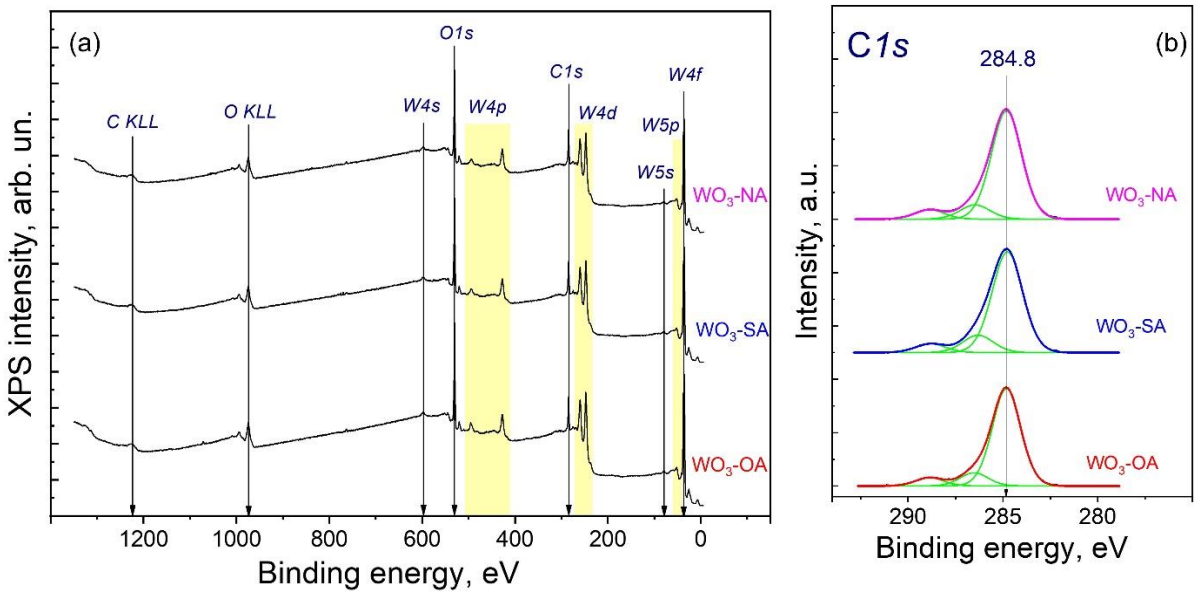

Figure S2. XPS survey (**a**) and C1s (**b**) spectra of WO_3-OA, WO_3-SA and WO_3-NA (**c**) samples.

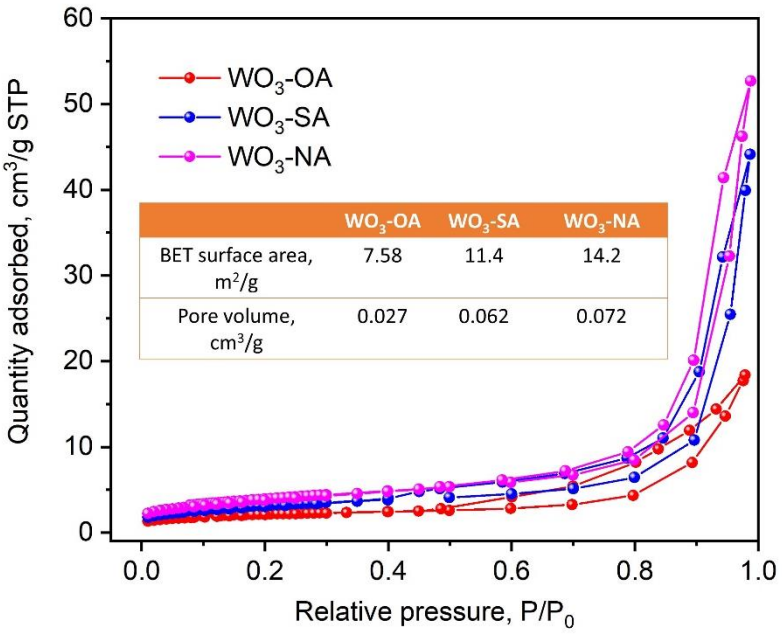

	WO_3-OA	WO_3-SA	WO_3-NA
BET surface area, m^2/g	7.58	11.4	14.2
Pore volume, cm^3/g	0.027	0.062	0.072

Figure S3. Nitrogen adsorption–desorption isotherms of WO_3-OA (**a**), WO_3-SA (**b**) and WO_3-NA (**c**) samples. Inset table shows the corresponding BET surface areas and pore volume values.

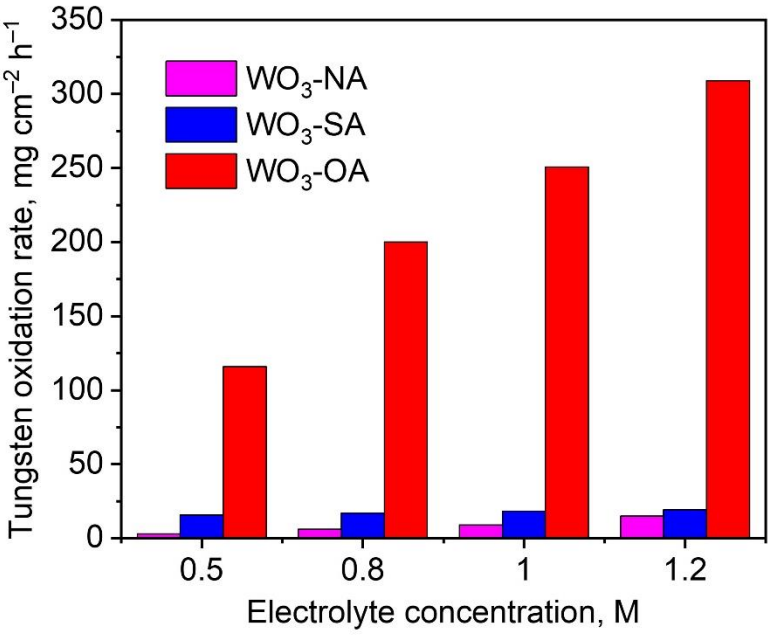

Figure S4. Effect of electrolyte concentration on tungsten electrochemical oxidation rate using different electrolytes.

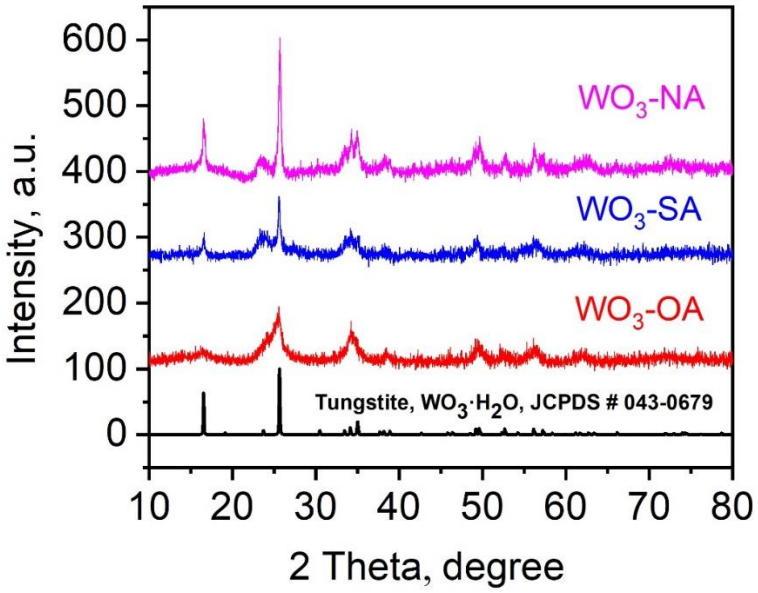

Figure S5. XRD patterns of the as-prepared powders by electrochemical oxidation of tungsten under pulse alternating current in comparison with the reference pattern of tungstite $WO_3 \cdot H_2O$.

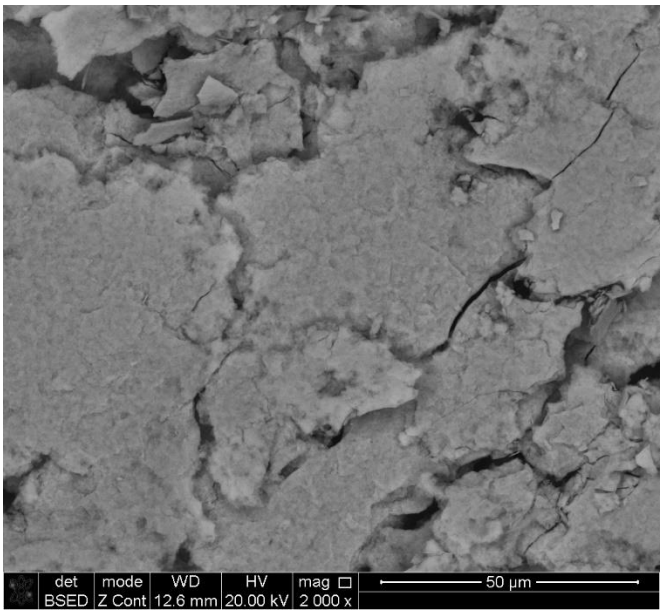

Figure S6. SEM image of the film structure obtained on tungsten electrode during electrochemical oxidation of W in oxalic acid under of pulse alternating current.

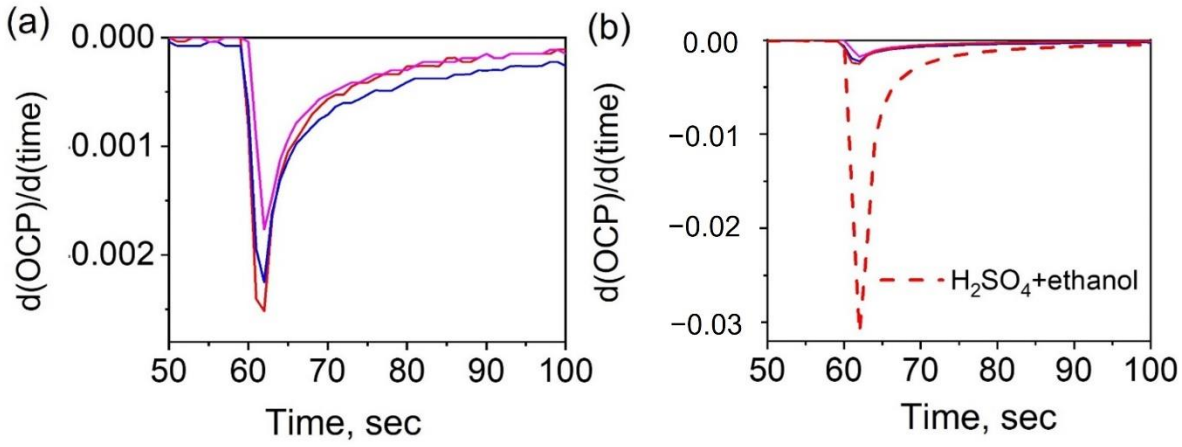

Figure S7. OCP decay derivative of d(OCP)/d(Time) vs. time curves of WO_3 samples in H_2SO_4 (**a**) and in H_2SO_4/ethanol (**b**) solution.

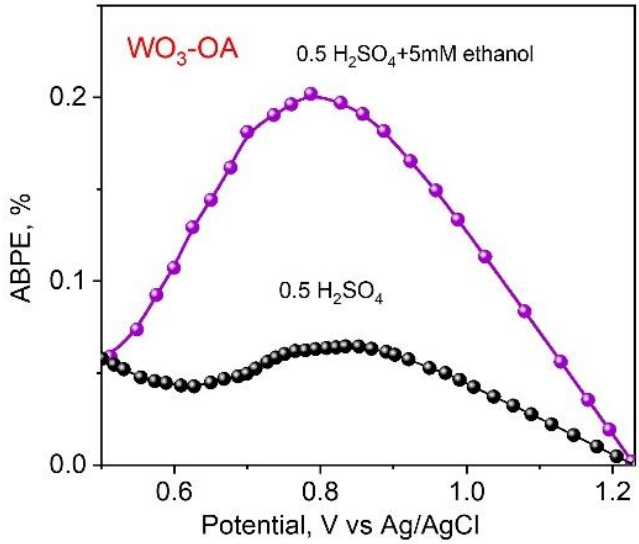

Figure S8. Applied bias photon-to-current efficiency (ABPE, %) as a function of applied potential for WO_3-OA sample.

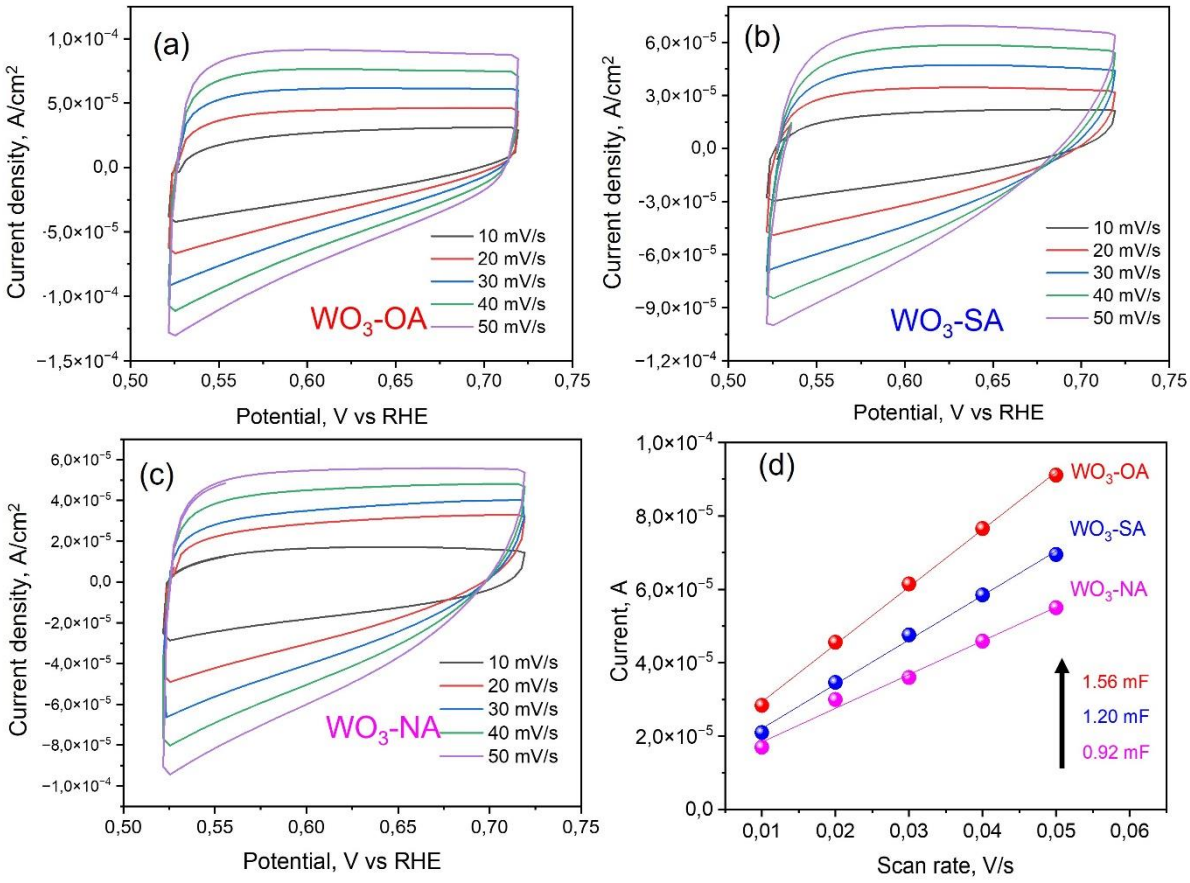

Figure S9. CVs at different scan rates in the potential range of 0.52–0.72 V vs the RHE (nonfaradaic region) in 0.5 M H_2SO_4 solution of (**a**) WO_3-OA, (**b**) WO_3-SA and (**c**) WO_3-NA, (**d**) Capacitive currents measured at 0.62 V vs the RHE as a function of scan rates.

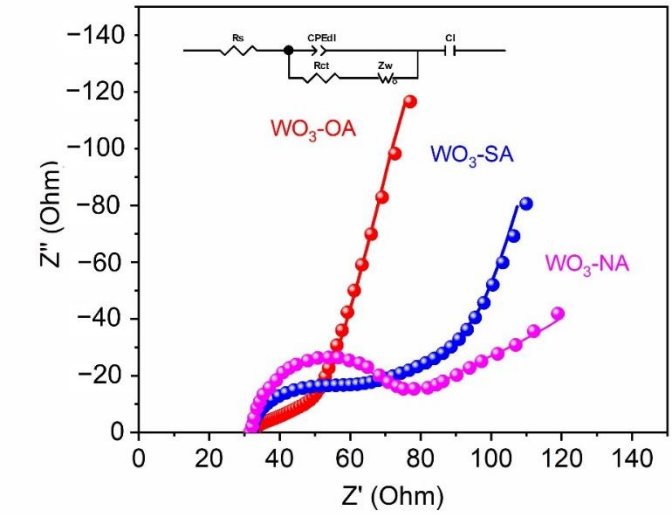

Figure S10. Nyquist plots of a WO_3 samples obtained in different electrolytes. The inset shows the equivalent circuit used for fitting the data with the resistances R_s and R_{ct}, the Warburg impedance Z_w, the constant phase element CPE_{dl} and the capacitance C_l.